


Article

Formulation and Characterization of Solid Lipid Nanoparticles Loaded with Troxerutin

Yahya F. Jamous^{1,*} , Najla A. Altwaijry^{2,*} , Mohamed T. S. Saleem³ , Aljoharah F. Alrayes², Sara M. Albishi² and Mashaal A. Almeshari²

¹ Vaccine and Bioprocessing Center, King Abdulaziz City for Science and Technology (KACST), Riyadh 12354, Saudi Arabia

² Department of Pharmaceutical Sciences, College of Pharmacy, Princess Nourah Bint Abdulrahman University, Riyadh 11564, Saudi Arabia; 438001400@pnu.edu.sa (A.F.A.); 438001699@pnu.edu.sa (S.M.A.); 438001245@pnu.edu.sa (M.A.A.)

³ College of Pharmacy, Riyadh ELM University, Riyadh 13244, Saudi Arabia; tsmohamed.saleem@riyadh.edu.sa

* Correspondence: yjamous@kacst.edu.sa (Y.F.J.); naaltwaijry@pnu.edu.sa (N.A.A.)

Abstract: Troxerutin (TXR), a naturally derived compound with diverse therapeutic potential, faces limitations in clinical efficacy due to poor bioavailability and rapid plasma clearance. This study focuses on troxerutin-loaded solid lipid nanoparticles (TXR-SLNs) and their physicochemical properties, intending to enhance drug release. TXR-SLNs were prepared via high-shear homogenization followed by ultrasonication, yielding optimized nanoparticles with an average size of 140.5 ± 1.02 nm, a uniform distribution (polydispersity index: 0.218 ± 0.01), and a stable emulsion (zeta potential: 28 ± 8.71 mV). The formulation exhibited 83.62% entrapment efficiency, indicating improved drug-loading capacity and extended drug release. Spectroscopic and thermodynamic analyses confirmed component compatibility. Despite a decline in entrapment efficiency induced by temperature after one month of storage at 23 °C, the formulation may retain acceptable stability. This study provides insight into SLNs as effective carriers for enhancing troxerutin's release profile, motivating further *in vivo* investigations to optimize therapeutic interventions.

Keywords: troxerutin; flavonoids; solid lipid nanoparticles; high-shear homogenization; drug release



Citation: Jamous, Y.F.; Altwaijry, N.A.; Saleem, M.T.S.; Alrayes, A.F.; Albishi, S.M.; Almeshari, M.A.

Formulation and Characterization of Solid Lipid Nanoparticles Loaded with Troxerutin. *Processes* **2023**, *11*, 3039. <https://doi.org/10.3390/pr11103039>

Academic Editors: Ibrahim M. Abu-Reidah and Evangelos Tsotsas

Received: 30 August 2023

Revised: 12 October 2023

Accepted: 19 October 2023

Published: 23 October 2023



Copyright: © 2023 by the authors. Licensee MDPI, Basel, Switzerland. This article is an open access article distributed under the terms and conditions of the Creative Commons Attribution (CC BY) license (<https://creativecommons.org/licenses/by/4.0/>).

1. Introduction

Flavonoids represent a class of polyphenolic compounds found abundantly in an extensive array of plants, fruits, vegetables, and leaves [1]. In recent times, these naturally occurring phytochemicals have garnered significant attention within modern medicine, where they have been harnessed to engender innovative therapeutic agents. This choice stems from their diverse and expansive biological activities, coupled with their remarkable health benefits, all achieved with a markedly low proclivity for eliciting side effects and toxicity [2]. Their repertoire encompasses compelling attributes, including antioxidative, anti-inflammatory, antimutagenic, and anticarcinogenic properties [3]. Moreover, flavonoids are known to modulate key cellular enzyme functions, such as cyclo-oxygenase (COX), lipoxygenase, and xanthine oxidase (XO) [1].

Empirical evidence has progressively accumulated, underscoring the pharmacological prowess of flavonoids in the context of diabetes. Their impact on promoting glycemic control and ameliorating lipid levels has garnered attention. This dual effect translates into a protective shield against a spectrum of complications, spanning nephropathy, neuropathy, hepatic impairments, and cardiovascular maladies [4,5]. El-Shiekh et al. [6] notably documented an exploration of the antibacterial and antiviral potential embedded within a plant-derived flavonoid.

Furthermore, an assortment of investigations have converged to emphasize the profound antioxidant properties exhibited by flavonoids. This quality plays a pivotal role in

mitigating oxidative stress, a factor intricately linked to the genesis of neurodegenerative diseases (NDDs) and neoplastic conditions [7–9].

Troloxerutin (TXR), also known as vitamin P4, belongs to the trihydroxyethyl group and is derived from the natural bioflavonoid rutin [10–13]. TXR stands as a promising natural compound renowned for its multifaceted pharmacological effects across diverse conditions [14]. Notably, numerous investigations have substantiated TXR's capacity to confer protection to vital organs such as the kidneys, liver, and brain, primarily through its robust ability to scavenge reactive oxidative species (ROS). This property is underpinned by its dual role as an antioxidant and anti-inflammatory agent [14–18].

Furthermore, TXR emerges as a key player in the management of vascular disorders, displaying a beneficial impact on blood fibrinolysis and erythrocyte aggregation [19,20]. These attributes position it as a compelling therapeutic option for addressing chronic venous insufficiency (CVI), a condition characterized by abnormal increases in erythrocyte aggregation and diminished pro-fibrinolytic activity [20].

In general, the application of TXR is constrained by its limited reabsorption following biliary excretion and suboptimal cell membrane penetration, consequently leading to swift plasma clearance and diminished bioavailability [13,21]. Additionally, the chemical configuration of TXR (Figure 1) contributes to its reduced bioavailability due to the presence of polyphenolic groups, which are susceptible to substantial *in vivo* degradation [1,22]. Nevertheless, the employment of nanoparticles presents a promising avenue for augmenting TXR's bioavailability, thereby enhancing its potential for achieving an improved therapeutic effect.

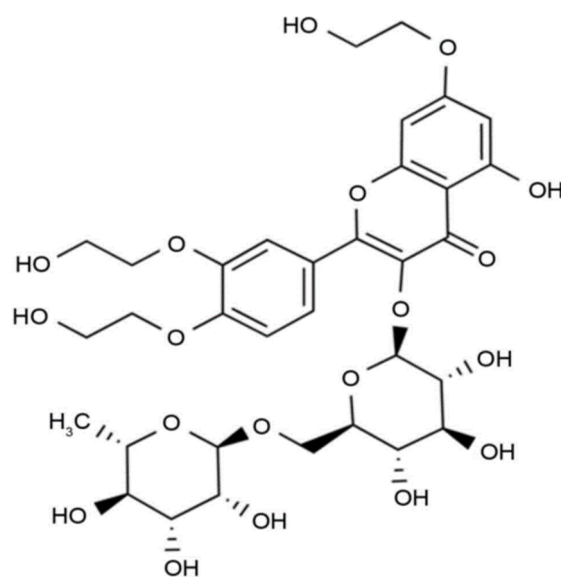


Figure 1. TXR's chemical structure.

In recent years, the realm of nanotechnology has experienced rapid expansion, emerging as a potent tool with extensive applications in medication delivery, diagnostics, cosmetics, and both biological and non-biological sciences [23]. However, the conventional delivery methods for therapeutic agents, including plant-derived flavonoids, are impeded by issues such as non-selectivity, low efficiency, and suboptimal bioavailability [24]. To surmount these limitations, the utilization of nanocarriers such as polymeric nanoparticles (NPs), liposomal NPs, and solid lipid NPs offers a promising avenue for optimizing drug delivery [24]. By enhancing the concentration of therapeutics at specific targets, these nanocarriers hold the potential to elevate efficacy, enhance biological system tolerability, and enable the utilization of lower dosages [24]. Furthermore, they offer the capacity to bolster the bioavailability of water-insoluble compounds [24]. The efficacy of nanocarriers

hinges on a multitude of factors, encompassing their physicochemical attributes, drug loading efficiency, drug release kinetics, and minimal toxicity [23].

Solid lipid nanoparticles (SLNs) represent a promising drug delivery system composed of active drug molecules, solid lipids, surfactants, and/or co-surfactants [10]. These nanoparticles can be safely formulated for diverse routes of administration, including oral, injectable, and topical applications [25]. The scope of SLN applications is extensive, offering the potential to enhance the treatment of various diseases through judicious physicochemical modifications [26]. Their versatility extends to loading both lipophilic and hydrophilic drugs, thereby improving the drug characteristics, extending action duration, and prolonging drug release profiles [27]. Consequently, this enables a reduction in administration frequency while concurrently enhancing therapeutic efficacy [27]. Beyond their ability to enhance drug oral bioavailability and sustain drug release, the heightened precision of drug targeting is a paramount advantage of SLNs when compared to conventional delivery methods [28].

Targeted drug delivery serves as a ubiquitous platform for all solid lipid nanoparticles, facilitating precise drug delivery to specific tissues or cells across various pathological contexts [29]. Through the integration of drugs into nanocarriers, solid lipid nanoparticles offer a novel paradigm for targeted drug delivery strategies [29]. As such, solid lipid nanoparticles emerge as a propitious avenue for the development of controlled and targeted drug delivery systems [29].

Recent studies have reported the potential pharmacological benefits of troxerutin-loaded nanoparticles by using various polymers like chitosan and selenium [30,31]. In the present study, we aimed to establish the application of TXR loading within nanoparticles by adopting simple methods. This study aimed to meticulously characterize the physicochemical properties and assess the drug release kinetics of troxerutin-loaded solid lipid nanoparticles (TXR-SLNs) through investigations. The loading process was facilitated using a combination of high-shear homogenization followed by ultrasonication. The physicochemical attributes, encompassing shape, size, polydispersity index, and zeta potential, were scrutinized using a zeta sizer instrument (Malvern, UK). Moreover, a comprehensive assessment was conducted through techniques including differential scanning calorimetry (DSC), transmission electron microscopy (TEM), and Fourier transform infrared (FTIR) spectroscopy to ascertain any alterations in crystal structure and potential chemical interactions between constituents. Concurrently, the study evaluated parameters such as drug entrapment efficiency (EE) and drug release profiles to comprehensively gauge the performance of the TXR-SLN formulation.

2. Methodology

2.1. Chemicals and Materials

Troxerutin (purity: 98%), soy lecithin, Tween-80, and a dialysis bag were procured from Solarbio, Beijing, China. Glyceryl behenate was acquired from Kejian Chem, Beijing, China. Absolute ethanol was obtained from Fisher Scientific UK Limited, Leicestershire, UK. Sodium phosphate dibasic was sourced from Sigma Aldrich, Saint Louis, MO, USA, while sodium phosphate monobasic anhydrous was obtained from ICN Biomedicals, Inc., Santa Ana, CA, USA.

2.2. Preparation of the TXR-SLNs

The methodology employed for the preparation of the TXR-SLNs was adapted from Tan et al. [32] with slight modifications. The synthesis of the TXR-SLNs involved a two-step process comprising high-shear homogenization followed by ultrasonication. Initially, Tween-80 was dissolved in 25 mL of distilled water and heated to 73 degrees Celsius (°C) using a water bath, resulting in the formation of an aqueous phase. Meanwhile, the lipid phase was created by dissolving TXR, soy lecithin, and glyceryl behenate in 5 mL of ethanol, which was then heated to 73 °C.

Subsequently, the aqueous phase was carefully introduced into the lipid phase. The resulting mixture underwent homogenization at 7000 rpm for 10 min utilizing a high-speed Ultra Turrax D-500 homogenizer (IKA T25, Germany) to establish an emulsion. This emulsion was further subjected to ultrasonication for 15 min using an ultrasonic cell crusher (Ningbo Biological Technology Co., Ltd., Ningbo, China), leading to the formation of a TXR-SLN emulsion. The emulsion was then stored at 4 °C.

For the formulation of TXR-SLNs, three distinct compositions involving varying quantities of Tween-80, soy lecithin, and glyceryl behenate were prepared as delineated in Table 1.

Table 1. The ingredient quantities of each prepared TXR-SLN formulation.

Formulation	Active Ingredient	Surfactant	Lipid Polymer	
	TXR	Tween-80	Glyceryl Behenate	Soy Lecithin
TXR-SLN 1	10 mg	500 µL	100 mg	50 mg
TXR-SLN 2	10 mg	250 µL	50 mg	50 mg
TXR-SLN 3	10 mg	500 µL	50 mg	100 mg

2.3. Characterization

2.3.1. Estimation of Particle Size, Polydispersity, and Zeta Potential

A dynamic light scattering technique using a zeta sizer (Malvern, UK) was employed to assess the average particle size, polydispersity index (PDI), and zeta potential [32] in the context of this research study. For DLS particle sizing, the sample needs to be water clear to very slightly hazy. If the solution is white or too hazy, it should be diluted further before attempting a DLS size measurement. Thus, before the measurement of particle size, PDI analysis, and zeta potential, the samples were appropriately diluted with distilled water at a ratio of 1:10. If the sample is too concentrated, the measured size of the particles will be inaccurate due to multiple scattering or viscosity effects. The subsequent examination was conducted at a fixed angle of 90° for particle size and 25 °C for zeta potential.

The determination of the average particle size, PDI, and zeta potential was carried out in triplicate to ensure accuracy and consistency.

2.3.2. Imaging by Transmission Electron Microscopy (TEM)

The surface morphology analysis of all formulations was conducted using transmission electron microscopy (TEM). To prepare the samples, a 15 min ultrasonication process was performed using bath sonication at room temperature. Subsequently, a single drop of the prepared formulations was carefully pipetted onto a Formvar/Carbon 400 mesh copper grid (Ted Pella, CA). The samples were left to air dry for 24 h at room temperature.

Visual observation and imaging were accomplished using a TEM instrument (Hitachi HD-2300A, Chicago, IL, USA), operating at an acceleration voltage of 200 kV.

2.3.3. Determination of the Entrapment Efficiency (EE)

The determination of entrapment efficiency involved quantifying the concentration of an untrapped substance within the aqueous solution after centrifugation. The prepared TXR-SLNs were subjected to centrifugation in a high-speed cooling centrifuge (Eppendorf, Hamburg, Germany) operating at 5000 rpm for 10 min, maintained at a temperature of 4 °C. Following centrifugation, the resultant sediment and supernatant liquid were carefully separated.

To assess the quantity of untrapped drug present in the supernatant, a UV-spectrophotometer (PerkinElmer, Waltham, MA, USA) was employed, utilizing a wavelength of 360 nm. This measurement facilitated the estimation of the percentage of entrapment efficiency.

The calculation of the percentage entrapment efficiency (%EE) was executed using the subsequent formula:

$$\%EE = \frac{\text{Total drug content} - \text{free drug}}{\text{Total drug content}} \times 100$$

2.3.4. Differential Scanning Calorimetry (DSC) Analysis

Differential scanning calorimetry (DSC) analysis was conducted to assess the physical state of the TXR-SLNs (Seiko Instruments Inc, Chiba, Japan). The procedure involved placing samples of TXR, blank SLNs, and TXR-SLNs into individual aluminum pans. An empty pan was utilized as a reference or control. The analysis was performed with a continuous flow of nitrogen gas. The temperature was incrementally increased from 20 to 300 °C, following a controlled rate of 10 °C per minute [32].

2.3.5. Fourier Transform Infrared (FTIR) Analysis

The Fourier transform infrared (FTIR-8400S, Shimadzu, Nakagyo-ku, Kyoto, Japan) technique was employed to elucidate interactions among the drug, surfactant, and lipid components. A total of five samples were meticulously prepared, comprising three solids and two liquids. The solid samples encompassed TXR, soy lecithin, and glyceryl behenate, while the liquid samples included TXR-SLNs and SLNs without TXR. The FTIR spectra were acquired using the conventional KBr disc/pellet methodology.

For the solid samples, a procedure involving grinding with anhydrous KBr powder and subsequent compression into pellets was carried out. In contrast, the liquid samples were directly applied onto the KBr window. The FTIR spectrum became accessible after a comprehensive scan and underwent subsequent analysis through software (LabSolutions IR, Shimadzu, Nakagyo-ku, Kyoto, Japan).

The FTIR spectra were meticulously recorded with a resolution of 4 cm⁻¹, spanning a range of 4000–400 cm⁻¹, and involved 50 scans.

2.3.6. Quantification of the Drug Release from the TXR-SLNs

To investigate the drug release of the TXR-SLNs, the dialysis bag method was employed, as described in [32]. A dialysis bag (catalog no. YA1070, flat width: 10 mm, molecular weight cut-off: 8000–14,000 Da, length: 5 m, Solarbio) was employed to facilitate controlled drug release. The dialysis bag was loaded with the three different TXR-SLN formulations, enabling the gradual release of the free drug into the surrounding media. The bag was immersed in distilled water for approximately 12 h to facilitate initial hydration.

Subsequently, 1 mL of each TXR-SLN formulation was separately introduced into three dialysis bags, securely fastened with clamps. Each bag was then placed within a conical flask containing 100 mL of phosphate-buffered saline (PBS; pH 7.4). These three conical flasks were positioned within a thermostatic shaker, maintaining a consistent environment for 48 h. At predetermined intervals, 1 mL of the buffer solution was sampled, with an equivalent volume of fresh PBS replenished into the conical flasks. The drug release profiles were assessed using a UV-Vis spectrophotometer at a wavelength of 360 nm, with distilled water serving as the blank sample. A similar procedure was executed for the control group, which consisted of TXR alone, to facilitate comparative analysis of the drug release.

The cumulative release of the TXR-SLNs was calculated using the following equation:

$$Q_n = C_n \times V_0 + (C_1 + C_2 + C_3 + \dots + C_n - 1) \times V$$

where:

V₀ represents the volume of the release medium;

Q_n denotes the cumulative release at the n-th sampling point;

C signifies the solution concentration;

C_n indicates the concentration at the n-th sampling point;

V stands for the volume of each sample.

The drug concentration in the formulations was determined using a calibration curve of TXR. A stock solution of TXR was prepared by dissolving it in 100 mL of double-distilled water at a concentration of 1 mg/mL. Subsequent working standards were prepared through dilution with a phosphate buffer of pH 7.4, resulting in concentrations of 0.5, 1, 5, 10, and 15 mg/mL. UV-Vis spectrophotometry was employed at a wavelength of 360 nm to quantify the drug concentration using the calibration curve. The entire procedure was conducted in triplicate, and the average absorbance was calculated. The calibration equation and R^2 value were subsequently determined and reported.

Drug release kinetics

The dissolution data were fitted to various equations, including zero-order (cumulative quantity of drug released vs. time), first-order (log cumulative proportion of drug remaining vs. time), Higuchi (cumulative proportion of drug released vs. square root of time), Hixson–Crowell (the cubic root of percent drug release vs. time), and Korsmeyer–Peppas (log cumulative proportion of drug released vs. log time), to elucidate the rate and mechanism of TXR release from the formulated samples. The in-house developed PSP-DISSO V2 software (Developed by BVDU's Poona College of Pharmacy, Pune, India) was employed to analyze the release kinetic parameters for the formulations in a phosphate buffer (pH 7.4). The correlation coefficients were calculated to assess data fit. The diffusion exponent (n) for different nanoparticles was determined, where $n \leq 0.45$ indicates Fickian (Case I) release, >0.45 but <0.89 suggests non-Fickian (anomalous) release, and >0.89 signifies super Case II release. In this context, Case II pertains to polymeric chain erosion, while anomalous transport (non-Fickian) refers to a combination of diffusion and erosion-controlled drug release [33].

2.3.7. Stability Studies

After measuring the initial particle size analysis of the three TXR-SLN formulations using the zeta sizer, the formulation samples were divided into two sets. One set was stored at 4 °C (in a refrigerator), and the second set was stored at room temperature (23 °C). All samples were kept in foil-sealed glass vials. Subsequently, the samples were retrieved at intervals of 5, 10, 20, and 30 days to assess particle size, polydispersity index, zeta potential, and entrapment efficiency.

3. Results

3.1. Drug Entrapment Efficiency (EE)

EE is a pivotal parameter for evaluating the drug-loading capacity of nanoparticles. The absorbance of each formulation was measured at 360 nm using a UV-Vis spectrophotometer and subsequently calculated through a calibration curve. As illustrated in Table 2, TXR-SLN 2 exhibited the highest EE, reaching 83.62%, in comparison to TXR-SLN 1 and TXR-SLN 3, with EEs of 76% and 77%, respectively.

Table 2. Entrapment efficiency (EE) of the TXR-SLN formulations.

S. No	Formulation Code	Entrapment Efficiency (%)
1	TXR-SLN 1	76.02
2	TXR-SLN 2	83.62
3	TXR-SLN 3	77.06

The entrapment was evaluated using a calibration curve depicted in Figure 2. The absorbance of each formulation was measured at 360 nm in phosphate-buffered saline (pH 6.8) using a UV-Vis spectrophotometer. A concentration–absorbance plot was generated, enabling the determination of the correlation coefficient and regression equation for TXR. Notably, the drug exhibited linearity across a concentration span of 0.5–15 mg/mL, with an R^2 value of 0.9992 for this concentration range.

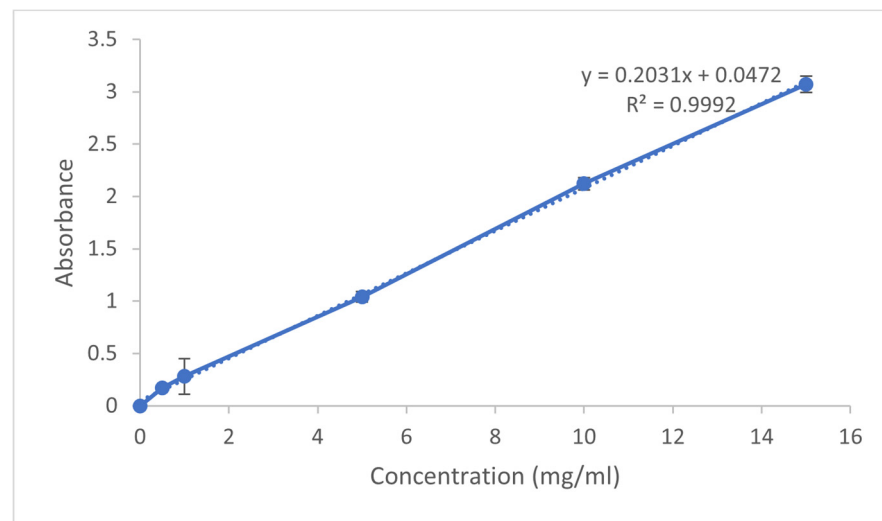


Figure 2. Calibration curve of TXR using a UV-Vis spectrophotometer (pH 6.8).

3.2. Measurement of Particle Size, Polydispersity Index (PDI), and Zeta Potential

The sizes of the three particles, PDI, and zeta potential were determined for the prepared samples. Among these, TXR-SLN 2 exhibited the smallest particle size, measuring at 140.5 ± 1.02 nm, and a PDI of 0.218 ± 0.01 (Table 3). The nanoparticle size and distribution of TXR-SLN 2 were notably favorable, as demonstrated in Figure 3. PDI values spanning from 0 to 0.5 indicate the presence of monodispersed and uniform materials. Furthermore, the zeta potential serves as an indicator of nanoparticle formulation stability by assessing surface charge and aggregation propensity. A zeta potential of ± 20 mV signifies a stabilized formulation. Remarkably, TXR-SLN 2 exhibited a zeta potential of 28.6 ± 8.71 mV, effectively contributing to the stability of the system (Table 3).

Table 3. Particle size, polydispersity index, and zeta potential of the formulations.

S. No	Formulation	Particle Size (nm)	Polydispersity Index (PDI)	Zeta Potential (mV)
1	TXR-SLN 1	349.9 ± 7.67	0.387 ± 0.06	14.9 ± 4.87
2	TXR-SLN 2	140.5 ± 1.02	0.218 ± 0.01	28.6 ± 8.71
3	TXR-SLN 3	152.5 ± 2.35	0.350 ± 0.02	12.6 ± 4.52

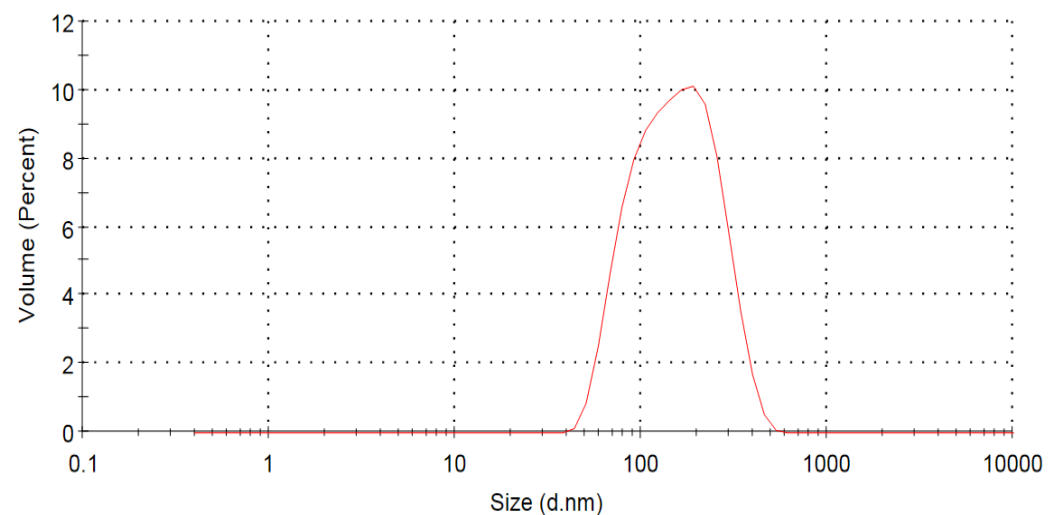


Figure 3. Particle size distribution of the TXR-SLN 2 formulation.

3.3. Transmission Electron Microscopy (TEM) Analysis

The shape and surface morphology of the optimal formulation were examined using TEM. The TEM micrograph depicts particles exhibiting a spherical shape, along with a smooth surface texture (Figure 4).

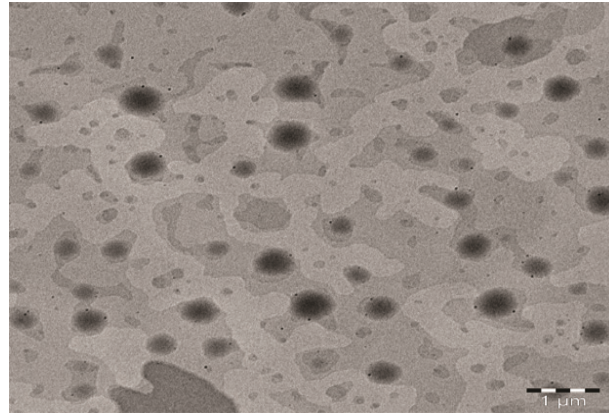


Figure 4. TEM micrograph of the TXR-SLN 2 formulation.

3.4. Fourier Transform Infrared Spectroscopy (FTIR)

A drug-excipient compatibility study was conducted using FTIR spectra, involving TXR and a TXR-excipient physical mixture. The outcomes are illustrated in Figure 5. The distinct peaks of troxerutin and those of its physical mixture reveal that the functional groups and characteristics of troxerutin remained unaltered. This observation indicates the absence of any interference from troxerutin solid lipid nanoparticles within the drug-excipient mixtures.

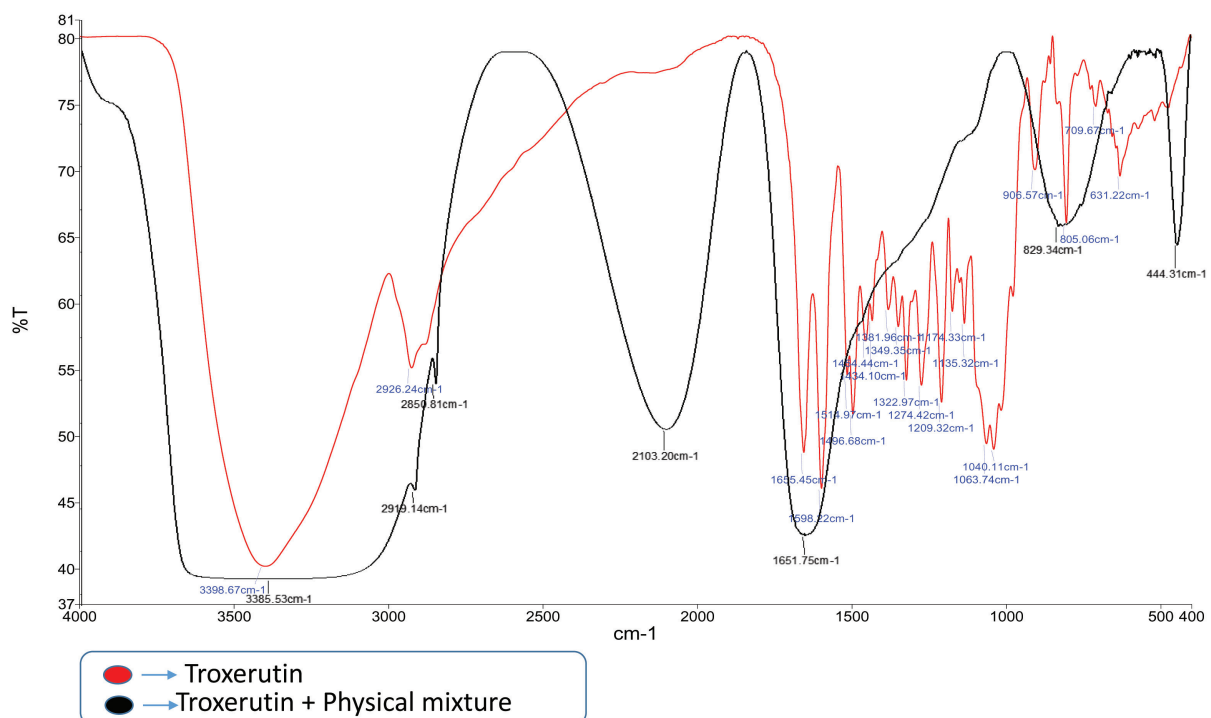


Figure 5. FTIR spectra of drug and excipient compatibility.

3.5. Differential Scanning Calorimetry (DSC)

The formulation of SLNs necessitated the validation of the expected physical state of the matrix lipid, which is of paramount importance. This validation can be achieved

through DSC. When comparing the DSC thermograms of the bulk lipids with those of the corresponding SLNs, notable differences in the signals' positions and shapes were often observed. Specifically, the DSC curve for TXR alone exhibited a sharp exothermic peak at 177.07 °C (with a ΔH of -39.33 mJ), corresponding to its known melting point of 181 °C. For the lipid component, the peak was observed at 110 °C. In the case of the SLN formulation, two distinct peaks emerged at 135 and 177.07 °C (Figure 6). The shifting of the lipid peak in the solid lipid nanoparticle formulation may be due to the lipid polymorphism.

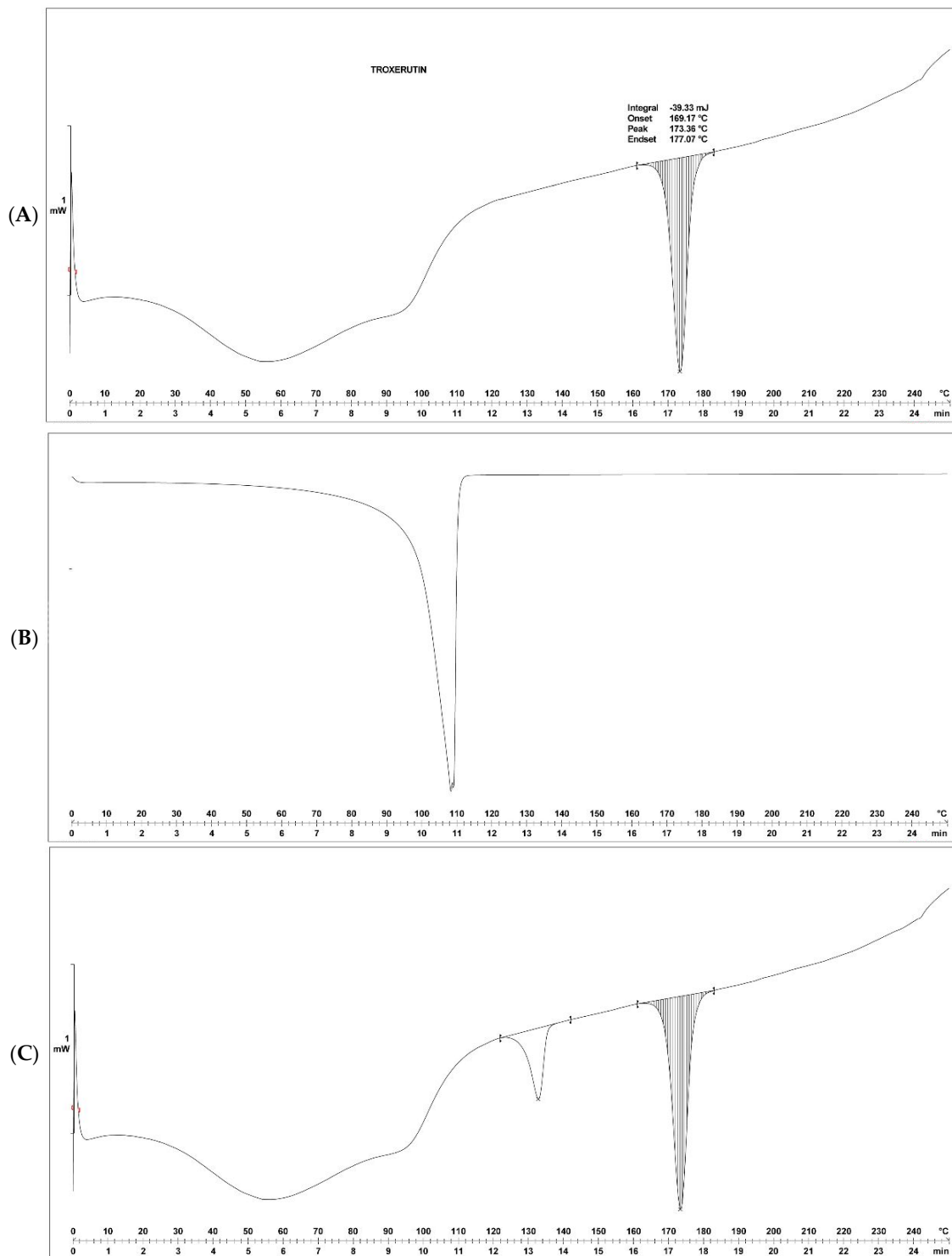


Figure 6. DSC spectra of the troxerutin (A), lipid (B), and SLN formulations (C).

3.6. Drug Release Study

The release profile of the TXR-SLNs, in comparison to TXR alone, is illustrated in Figure 7. All formulations demonstrated sustained drug release over 24 h in a phosphate-buffered saline medium. Within the same release medium, the cumulative drug release for all three formulations was more pronounced during the initial 4 h period. Notably, the TXR-SLN 2 formulation displayed the highest cumulative drug release at 24 h, reaching 82.47%. Conversely, TXR-SLN 1 exhibited a 56.33% drug release, and TXR-SLN 3 displayed a 66.51% release within the same timeframe. As for TXR alone, its maximum cumulative drug release occurred at 2 h. Comparatively, the TXR-SLNs exhibited elevated cumulative drug release over extended intervals in contrast to TXR alone. For a comprehensive overview, the dissolution data are presented in Table 4.

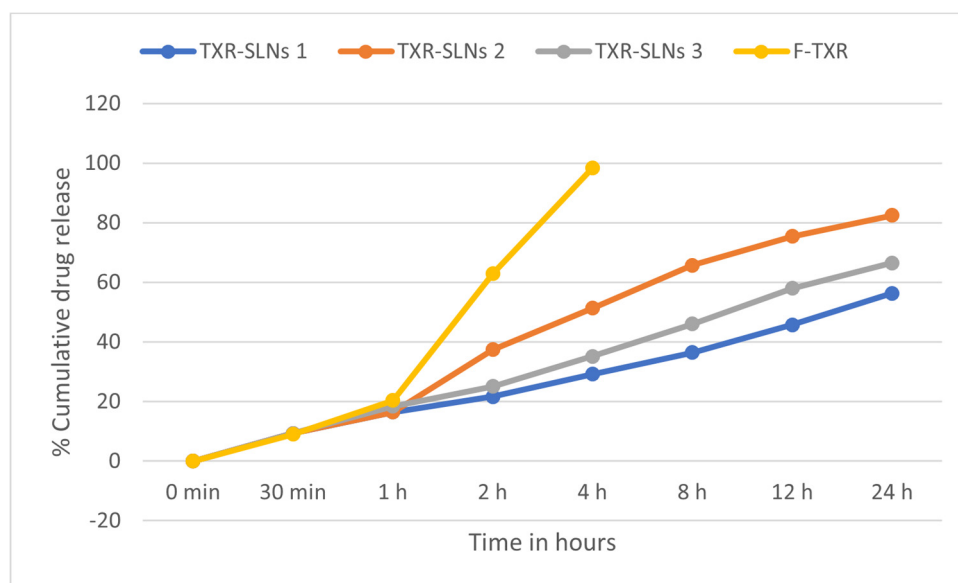


Figure 7. Percentage of cumulative drug release of the TXR-loaded SLNs.

Table 4. Percentage of cumulative drug release of the TXR-SLN dissolution data.

Time	% Cumulative Drug Released \pm SD ($n = 3$)			
	TXR-SLN 1	TXR-SLN 2	TXR-SLN 3	F-TXR
0 min	0	0	0	0
30 min	9.36 \pm 0.14	9.36 \pm 0.83	9.36 \pm 0.97	9.05 \pm 0.64
1 h	16.46 \pm 0.48	16.46 \pm 0.93	18.45 \pm 0.88	20.38 \pm 0.37
2 h	21.65 \pm 0.92	37.43 \pm 0.47	25.05 \pm 0.17	62.86 \pm 0.29
4 h	29.17 \pm 0.77	51.38 \pm 0.84	35.19 \pm 0.44	98.36 \pm 0.47
8 h	36.47 \pm 0.46	65.71 \pm 0.64	46.02 \pm 0.65	--
12 h	45.72 \pm 0.13	75.45 \pm 0.54	57.95 \pm 0.66	--
24 h	56.33 \pm 0.67	82.47 \pm 0.16	66.51 \pm 0.89	--

3.7. TXR Release Kinetic Study

The kinetics and mechanism of drug release were evaluated for the prepared SLNs. The release profiles of the formulations were scrutinized by fitting them to various equations, including zero-order, first-order, Higuchi, and Korsmeyer–Peppas. Among these, the optimal formulation underwent in-depth analysis to determine the underlying drug release mechanism. In these experiments, the release profile of TXR-SLN 2 exhibited substantial linearity, evident from a regression value of 0.916. This finding indicates that the drug

release adhered to Higuchi's equation, thereby confirming diffusion as the primary driver of drug release. To validate the diffusion mechanism, the dissolution data were also subjected to fitting the Korsmeyer–Peppas equation, resulting in a slope (n) value of 0.95. A comprehensive presentation of these results is provided in Table 5 and Figure 8 below.

Table 5. Kinetic release study of TXR-SLN 2.

Zero-Order	First-Order	Higuchi	Korsmeyer–Peppas	
R^2	R^2	R^2	R^2	N
0.6993	0.8714	0.916	0.567	0.95

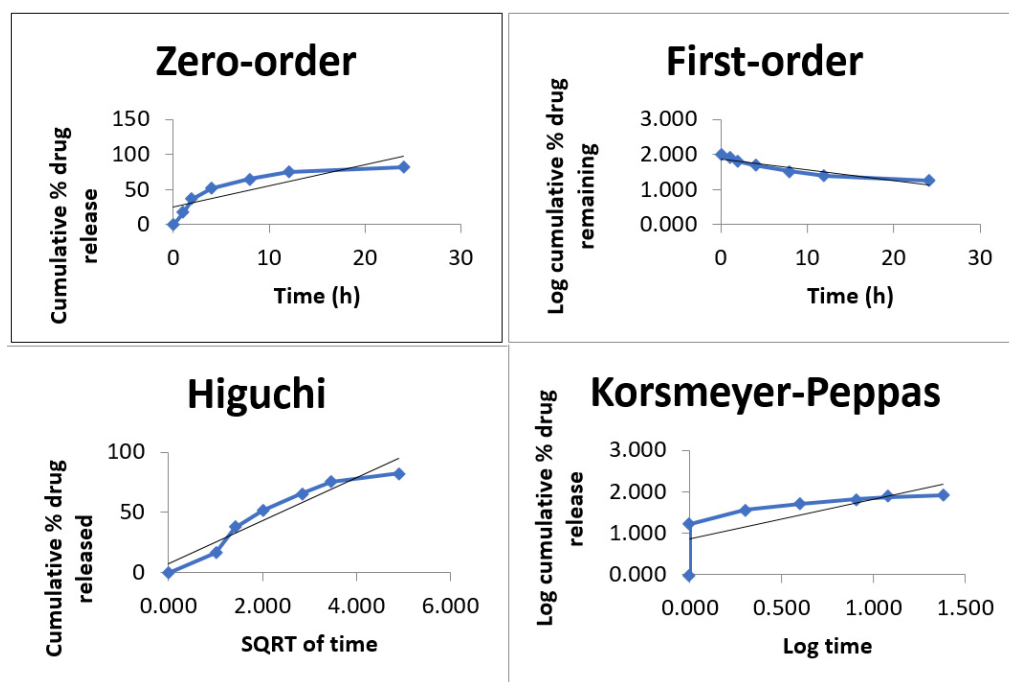


Figure 8. Release kinetic study of TXR-SLN 2.

3.8. Stability Studies

The results of the particle size, PDI, and zeta potential measurements for the three formulations after one month of refrigerated storage (4 °C) indicate minimal differences when compared to the measurements taken on the first day immediately after preparation. However, the particle size, PDI, and zeta potential for TXR-SLN 2 remained superior to those of TXR-SLN 1 and TXR-SLN 3, as illustrated in Table 6.

Table 6. Results of the particle size, polydispersity index (PDI), and zeta potential measurements for the three formulations after one month of refrigerated storage (4 °C).

S. No	Formulation	Particle Size (nm)	Polydispersity Index (PDI)	Zeta Potential (mV)
1	TXR-SLN 1	360.9 ± 6.10	0.391 ± 0.05	16 ± 3.48
2	TXR-SLN 2	151 ± 2.03	0.221 ± 0.03	28.4 ± 5.32
3	TXR-SLN 3	155.5 ± 2.05	0.356 ± 0.03	14.5 ± 4.31

The results of the particle size, PDI, and zeta potential measurements for the three formulations after one month of room-temperature storage (23 °C) indicate minimal differences when compared to the measurements taken on the first day immediately after

preparation. However, the particle size, PDI, and zeta potential for TXR-SLN 2 remained superior to those of TXR-SLN 1 and TXR-SLN 3, as illustrated in Table 7.

Table 7. Results of the particle size, polydispersity index (PDI), and zeta potential measurements for the three formulations after one month of room-temperature storage (23 °C).

S. No	Formulation	Particle Size (nm)	Polydispersity Index (PDI)	Zeta Potential (mV)
1	TXR-SLN 1	382 ± 5.23	0.392 ± 0.02	14 ± 2.13
2	TXR-SLN 2	154 ± 3.01	0.221 ± 0.02	28.2 ± 3.21
3	TXR-SLN 3	162.5 ± 2.03	0.371 ± 0.04	13.1 ± 3.11

The results of the EE identification for the three TXR-SLN formulations after one month of refrigerated storage (4 °C) indicate a slight decrease in entrapment efficiency compared to the same formulations immediately after preparation on the first day, as illustrated in Table 8.

Table 8. Entrapment efficiency (EE) of the TXR-SLN formulations after one month of refrigerated storage (4 °C).

S. No	Formulation Code	Entrapment Efficiency (%)
1	TXR-SLN 1	71.23619
2	TXR-SLN 2	77.54231
3	TXR-SLN 3	73.23486

The results of the EE identification for the three TXR-SLN formulations after one month of room-temperature storage (23 °C) indicate a significant decrease in entrapment efficiency compared to the same formulations immediately after preparation on the first day. However, the EE of TXR-SLN 2 was still within the normal range for stability determination, as illustrated in Table 9.

Table 9. Entrapment efficiency (EE) of the TXR-SLN formulations after one month of room-temperature storage (23 °C).

S. No	Formulation Code	Entrapment Efficiency (%)
1	TXR-SLN 1	54.36215
2	TXR-SLN 2	71.32457
3	TXR-SLN 3	45.23615

4. Discussion

The impact of lipids on SLNs entails a highly intricate interplay. Notably, the presence of lipid molecules with longer chains and the heightened viscosity within the oil phase can culminate in the generation of larger particle sizes. It is essential to acknowledge that the imperfections stemming from the complex nature of lipid materials and their imperfect crystal structures can also contribute to EE [25,34].

In the context of our current study, we opted to employ glyceryl behenate as the solid lipid polymer. Characterized as a fusion of glycerol esters and behenic acid, glyceryl behenate predominantly comprises glyceryl behenate. This intricate lipid entity further encompasses an array of mono-, di-, and triglycerides, each marked by distinct chain lengths. This amalgamation of diverse components imparts an irregularity on the crystal lattice, thereby fostering an environment conducive to the assimilation of bioactive compounds.

Consequently, this intricate structural composition not only enhances compatibility, but also elevates the efficacy of the formed SLNs [25,34,35].

Surfactants play a pivotal role in shaping the ideal configuration of SLNs, wielding a range of beneficial effects by inducing surface property modifications. These modifications encompass a reduction in surface tension, facilitating particle dispersion, mitigating particle aggregation, and enhancing the stability of the SLN emulsion [36,37]. It is noteworthy that the influence of surfactants is not confined solely to surface properties; their impact extends to the degree of lattice order, contributing significantly to nanoparticle stability [25,36,37].

In the context of our investigation, we purposefully incorporated soy lecithin and Tween-80 as both surfactants and co-surfactants. This deliberate selection was underpinned by their demonstrated capability to yield a multitude of favorable results. Notably, this encompasses the achievement of reduced particle dimensions, elevated EE, and enhanced overall stability [25,36]. This judicious choice of surfactants not only seeks to fine-tune the system for optimal performance, but also harmonizes seamlessly with our overarching goal of engineering SLNs endowed with exceptional attributes.

The methodology employed in this study to design SLNs encompassed a two-step process: High-shear homogenization succeeded by ultrasonication. This combined approach stands out as a straightforward, dependable, and feasible technique renowned for SLN preparation [25]. The initial phase of homogenization yielded a stable and lucid dispersion of SLNs, characterized by an appropriate particle size. However, it is noteworthy that this process, due to its elevated speed, could inadvertently introduce a profusion of bubbles and atomization.

To circumvent such limitations, the subsequent step involved harnessing ultrasonication. This strategic inclusion was designed to mitigate the issues stemming from high-shear homogenization. The ultrasonication force proved instrumental in homogenizing the dispersion of the formulation, thereby rectifying the anomalies induced by the prior high-shear homogenization process [38]. This orchestrated combination of techniques not only yielded clear benefits in terms of stability and particle uniformity, but also highlighted the intricacies involved in optimizing SLN fabrication.

Physicochemical characteristics, such as particle size, PDI, and zeta potential, hold paramount importance as attributes of lipid nanocarriers. These characteristics exert substantial influence over multiple facets, including drug stability, entrapment efficiency, drug release kinetics, biodistribution, and cellular uptake. Notably, in the realm of nanoscale systems, size stability assumes heightened significance when juxtaposed with their microscale counterparts. This distinction arises from the vast specific surface area inherent to nanoscale systems, a factor that distinguishes them from their microscale counterparts [39].

As the radius of the sphere and particle size decrease, there is a consequential elevation in the surface area-to-volume ratio [40]. This fundamental geometric principle invariably underscores the fact that diminutive particle dimensions yield a proportionally larger surface area concerning the volume. It is within this interplay that the foundation for a host of nanoscale system properties is established [40].

In this study, the optimal formulation was TXR-SLN 2. The selection of TXR-SLN 2 was based on its particle size, PDI, and zeta potential values. The particle size measured 140.5 ± 1.02 nm, with a PDI of 0.218 ± 0.01 and a zeta potential of 28.6 ± 8.71 . A PDI value of 0.3 or below in lipid-based nanocarriers is considered acceptable, indicating a homogeneous population [36]. The zeta potential range of 28.6 ± 8.71 , which is close to 30, suggests good stability [38]. Maintaining a constant and narrow size distribution is crucial for achieving optimal clinical outcomes with nanocarrier formulations [39]. The size and polydispersity index in the present study was comparatively less than the recently published work with chitosan-loaded troxerutin nanoparticles, in which the size and polydispersity index was 692 d-nm and 0.355, respectively [30]. Both particle size and PDI were expected to increase with the addition of lipid components to the formulations [41,42]. TXR-SLN 2 contained fewer lipid polymers compared to the other formulations, resulting in a monodispersed distribution and smaller size.

The EE of the three formulations was evaluated by measuring absorbance using a UV-Vis spectrophotometer and then plotted on a calibration curve (Figure 2). The results further support the identification of TXR-SLN 2 as the best formulation, exhibiting the highest EE value of 83.62%. The entrapment efficiency percentage was increased as the sonication time increased from 5 to 15 min [43]. A higher entrapment efficiency (83.62%) was achieved when TXR-SLN 2 was processed by ultrasonication for 15 min, compared to the other two formulations. The optimal formulation displayed an increased EE attributed to the lower soy lecithin and surfactant concentrations, as well as fewer lipid polymers, all of which contributed to a smaller particle size.

FTIR is a technique used to elucidate the chemical composition of various organic chemicals, polymers, and other materials [44]. The measurements were conducted to identify the potential biomolecules responsible for capping and effectively stabilizing the TXR-SLNs [44]. The FTIR analysis in this study revealed characteristic peaks present in both TXR alone and the TXR-SLNs. The results demonstrated that there were no missing functional peaks in the formulated TXR-SLNs. Furthermore, the formulation exhibited no significant physicochemical interactions between the drug and lipid.

The DSC technique measures the disparity in heat flux delivered to a test sample and a reference sample at the same temperature [45]. This makes it possible to quantify the differences in heat flows resulting from sample melting, crystallization, chemical reactions, or evaporation [45]. The DSC curve of TXR alone displayed a sharp exothermic peak at 177.07 °C ($\Delta H = -39.33$ mJ), corresponding to its melting point of 181 °C. For the lipid, the peak was observed at 110 °C, while for the SLN formulation, two peaks were identified at 135 and 177.07 °C. Both TXR alone and the SLNs exhibited the same exothermic peak at 177.07 °C. DSC offers insights into the characteristics and temperature parameters of individual samples [45], thus enhancing the quality and physicochemical properties of the product during various technological processes involving TXR-SLNs [45].

The release profile of the TXR-SLNs was tested. Seven samples were taken from all three formulations, and their cumulative drug release was measured. All formulations successfully released the drug in a sustained manner over 24 h in a phosphate-buffered saline solution. Among the formulations, TXR-SLN 2 exhibited the highest cumulative drug release at 24 h, reaching 82.47%. In contrast, TXR alone displayed the maximum cumulative drug release within 2 h. The TXR-SLNs demonstrated higher cumulative drug release over extended periods compared to TXR alone.

The main lipid components used were glyceryl behenate, soy lecithin, and Tween-80 as surfactants. Tween-80 contributed to both the stability and improved bioavailability of the SLNs by acting as a permeability enhancer [46]. Furthermore, it can increase intestinal permeability while reducing the activity of intestinal efflux transporters, including P-glycoprotein efflux pump activity [46]. The primary factor influencing oral absorption and bioavailability is intestinal efflux by P-glycoprotein and other transporters [46].

The release kinetic study demonstrated the drug release behavior of the SLNs. The formulations were evaluated by fitting the drug release profiles to various equations, including the zero-order, first-order, Higuchi, and Korsmeyer–Peppas models [47]. The optimal formulation, TXR-SLN 2, exhibited a better fit to Higuchi's model, which characterizes drug release from polymeric systems and aids in understanding the release mechanism and comparing differences among formulations [48,49]. A release exponent (n) greater than 0.89 indicates super Case II transport, involving drug release through both diffusion and relaxation of the SLNs. For the optimized formulation, TXR showed a predominant mechanism of super Case II transport.

Additionally, an R^2 value of 0.916 came closest to 1. Both the SLN formulations and the drug release were time-dependent. Consequently, TXR-SLN 2 achieved the highest in vitro release concentration around 24 h. These findings are consistent with the drug release results.

TEM is employed in cell biology, involving the imaging of stained thin sections of plastic-embedded cells by passing an electron beam through the sample. This process

causes the electrons to be absorbed and scattered, creating contrast and generating an image [50]. The results indicated that the TXR-SLNs were spherical with a smooth surface, indicative of the material's natural tendency to minimize its energy state [51].

The one-month stability study for the three formulations, measured by particle size, PDI, zeta potential, and EE, indicated minimal differences under both conditions (4 and 23 °C). However, a significant reduction in entrapment efficiency was observed after one month at 23 °C, suggesting a negative impact of temperature on the stability of the formulations over time. Notably, the stability study of TXR-SLN 2 remained within the acceptable stability range, distinguishing it from both TXR-SLN 1 and TXR-SLN 1.

This study has some potential limitations. First, there is a need for further optimization or factorial design. A factorial design could have assisted in examining how multiple factors affect a dependent variable, both individually and collectively. Evaluation of the toxicity of nanomaterials is essential to identify the effect of the nanomaterials used in the formulation during in vivo animal or human studies [52]. Additionally, this study employed a limited number of formulations, preventing us from anticipating potential variations in results across different formulations. Moreover, the use of a single surfactant and lipid polymer raises questions about the effectiveness of employing alternative surfactants or lipid polymers.

5. Conclusions

TXR-SLNs were prepared through high-shear homogenization followed by ultrasonication, and the formulation was optimized using CCD-RSM. The results of the drug release study indicated that the cumulative amount of drug released from the TXR-SLNs was significantly higher compared to that from TXR alone, reaching 82.47% within 24 h. This suggests that TXR-SLNs can enhance the drug release profile of TXR. Moreover, the kinetic investigation of drug release from TXR-SLN 2 revealed a combination of diffusion and relaxation mechanisms.

However, future plans involve in vivo drug release and efficacy studies for determining the performance of an optimal TXR-SLN formulation, along with toxicity evaluation of nanomaterials of the formulation.

Author Contributions: Conceptualization: Y.F.J., N.A.A. and M.T.S.S.; methodology: A.F.A., S.M.A. and M.A.A.; formal Analysis: Y.F.J., N.A.A. and M.T.S.S.; investigation: Y.F.J., N.A.A. and M.T.S.S.; writing, reviewing, and editing: Y.F.J., N.A.A., M.T.S.S., A.F.A., S.M.A. and M.A.A.; supervision: Y.F.J., N.A.A. and M.T.S.S. All authors have read and agreed to the published version of the manuscript.

Funding: This research was funded by grants from the Princess Nourah bint Abdulrahman University Researchers Supporting Project (grant number, PNURSP2023R98), Princess Nourah bint Abdulrahman University, Riyadh, Saudi Arabia.

Data Availability Statement: All of the data are included in the manuscript.

Acknowledgments: The authors would like to thank King Abdulaziz City for Science and Technology (KACST), Riyadh, Saudi Arabia.

Conflicts of Interest: The authors declare no conflict of interest.

Abbreviations

COX: Cyclo-oxygenase; CVI: Chronic venous insufficiency; DSC: Differential scanning calorimetry; EE: Entrapment efficiency; FTIR: Fourier transform infrared spectroscopy; NDDs: Neurodegenerative diseases; NPs: Nanoparticles; pH: Potential of hydrogen; Q_n: Cumulative release at the n-th sampling point; ROS: Reactive oxidative species; R²: Coefficient of determination; rpm: Revolutions per minute; SLNs: Solid lipid nanoparticles; TEM: Transmission electron microscopy; TXR: Troxerutin; TXR-SLNs: Troxerutin-loaded solid lipid nanoparticles; UV: Ultraviolet; XO: Xanthine oxidase; °C: Degrees Celsius.

References

1. Ullah, A.; Munir, S.; Badshah, S.L.; Khan, N.; Ghani, L.; Poulson, B.G.; Emwas, A.H.; Jaremko, M. Important Flavonoids and Their Role as a Therapeutic Agent. *Molecules* **2020**, *25*, 5243. Available online: <https://www.ncbi.nlm.nih.gov/pmc/articles/PMC7697716/> (accessed on 24 September 2022). [CrossRef]
2. Abbaszadeh, F.; Fakhri, S.; Khan, H. Targeting apoptosis and autophagy following spinal cord injury: Therapeutic approaches to polyphenols and candidate phytochemicals. *Pharmacol. Res.* **2020**, *160*, 105069. Available online: <https://pubmed.ncbi.nlm.nih.gov/32652198/> (accessed on 25 September 2022). [CrossRef]
3. Kozłowska, A.; Szostak-Wegierek, D. Flavonoids—Food sources and health benefits. *Rocz. Panstw. Zakł. Hig.* **2014**, *65*, 79–85. Available online: <https://pubmed.ncbi.nlm.nih.gov/25272572/> (accessed on 24 September 2022). [PubMed]
4. Ghorbani, A. Mechanisms of antidiabetic effects of flavonoid rutin. *Biomed. Pharmacother.* **2017**, *96*, 305–312. Available online: <https://pubmed.ncbi.nlm.nih.gov/29017142/> (accessed on 25 September 2022). [CrossRef] [PubMed]
5. Mahmoud, A.M.; Hernández Bautista, R.J.; Sandhu, M.A.; Hussein, O.E. Beneficial Effects of Citrus Flavonoids on Cardiovascular and Metabolic Health. *Oxidative Med. Cell. Longev.* **2019**, *2019*, 5484138. Available online: <https://www.ncbi.nlm.nih.gov/pmc/articles/PMC6431442/> (accessed on 6 August 2022). [CrossRef] [PubMed]
6. El-Shiekh, R.A.; Abdelmohsen, U.R.; Ashour, H.M.; Ashour, R.M. Novel Antiviral and Antibacterial Activities of Hibiscus schizopetalus. *Antibiotics* **2020**, *9*, 756. Available online: <https://www.ncbi.nlm.nih.gov/pmc/articles/PMC7692239/> (accessed on 6 August 2022). [CrossRef]
7. Kopustinskiene, D.M.; Jakstas, V.; Savickas, A.; Bernatoniene, J. Flavonoids as Anticancer Agents. *Nutrients* **2020**, *12*, 457. Available online: <https://www.ncbi.nlm.nih.gov/pmc/articles/PMC7071196/> (accessed on 6 August 2022). [CrossRef]
8. Hussain, G.; Zhang, L.; Rasul, A.; Anwar, H.; Sohail, M.U.; Razzaq, A.; Aziz, N.; Shabbir, A.; Ali, M.; Sun, T. Role of Plant-Derived Flavonoids and Their Mechanism in Attenuation of Alzheimer's and Parkinson's Diseases: An Update of Recent Data. *Mol. A J. Synth. Chem. Nat. Prod. Chem.* **2018**, *23*, 814. Available online: <https://www.ncbi.nlm.nih.gov/pmc/articles/PMC6017497/> (accessed on 6 August 2022). [CrossRef]
9. de Andrade, R.B.T.; Diniz, T.C.; Pinto, T.C.C.; de Oliveira, R.G.; e Silva, M.G.; de Lavor, É.M.; Fernandes, A.W.C.; de Oliveira, A.P.; de Almeida, F.P.R.; da Silva, A.A.M.; et al. Flavonoids as Therapeutic Agents in Alzheimer's and Parkinson's Diseases: A Systematic Review of Preclinical Evidence. *Oxidative Med. Cell. Longev.* **2018**, *2018*, 7043213. Available online: <https://www.ncbi.nlm.nih.gov/pmc/articles/PMC5971291/> (accessed on 6 August 2022). [CrossRef]
10. Rajpoot, K. Solid Lipid Nanoparticles: A Promising Nanomaterial in Drug Delivery. *Curr. Pharm. Des.* **2019**, *25*, 3943–3959. Available online: <https://pubmed.ncbi.nlm.nih.gov/31481000/> (accessed on 13 July 2022). [CrossRef]
11. Shu, L.; Zhang, W.; Huang, C.; Huang, G.; Su, G. Troxerutin Protects Against Myocardial Ischemia/Reperfusion Injury Via Pi3k/Akt Pathway in Rats. *Cell Physiol. Biochem.* **2017**, *44*, 1939–1948. Available online: <https://pubmed.ncbi.nlm.nih.gov/29241161/> (accessed on 12 July 2022). [CrossRef] [PubMed]
12. Yu, Z.P.; Yu, H.Q.; Li, J.; Li, C.; Hua, X.; Sheng, X.S. Troxerutin attenuates oxygen-glucose deprivation and reoxygenation-induced oxidative stress and inflammation by enhancing the PI3K/AKT/HIF-1 α signaling pathway in H9C2 cardiomyocytes. *Mol. Med. Rep.* **2020**, *22*, 1351–1361. Available online: <https://pubmed.ncbi.nlm.nih.gov/32626962/> (accessed on 24 September 2022). [CrossRef] [PubMed]
13. Xin, X.; Zhang, M.; Li, X.; Lai, F.; Zhao, G. Biocatalytic synthesis of acylated derivatives of troxerutin: Their bioavailability and antioxidant properties in vitro. *Microb. Cell Fact.* **2018**, *17*, 130. Available online: <https://microbialcellfactories.biomedcentral.com/articles/10.1186/s12934-018-0976-x> (accessed on 24 September 2022). [CrossRef] [PubMed]
14. Zamanian, M.; Bazmandegan, G.; Sureda, A.; Sobarzo-Sanchez, E.; Yousefi-Manesh, H.; Shirooie, S. The Protective Roles and Molecular Mechanisms of Troxerutin (Vitamin P4) for the Treatment of Chronic Diseases: A Mechanistic Review. *Curr. Neuropharmacol.* **2021**, *19*, 97. Available online: <https://www.ncbi.nlm.nih.gov/pmc/articles/PMC7903491/> (accessed on 24 September 2022). [CrossRef]
15. Shan, Q.; Zheng, G.; Han, X.; Wen, X.; Wang, S.; Li, M.; Zhuang, J.; Zhang, Z.F.; Hu, B.; Zhang, Y.; et al. Troxerutin Protects Kidney Tissue against BDE-47-Induced Inflammatory Damage through CXCR4-TXNIP/NLRP3 Signaling. *Oxid. Med. Cell. Longev.* **2018**, *2018*, 9865495. Available online: <https://www.ncbi.nlm.nih.gov/pmc/articles/PMC5932985/> (accessed on 24 September 2022). [CrossRef]
16. Shan, Q.; Zhuang, J.; Zheng, G.; Zhang, Z.; Zhang, Y.; Lu, J.; Zheng, Y. Troxerutin Reduces Kidney Damage against BDE-47-Induced Apoptosis via Inhibiting NOX2 Activity and Increasing Nrf2 Activity. *Oxid. Med. Cell. Longev.* **2017**, *2017*, 6034692. Available online: <https://www.ncbi.nlm.nih.gov/pmc/articles/PMC5661100/> (accessed on 24 September 2022). [CrossRef]
17. Zhang, Z.F.; Shao-Hua, F.A.N.; Zheng, Y.L.; Jun, L.U.; Dong-Mei, W.U.; Shan, Q.U.N.; Hu, B. Troxerutin protects the mouse liver against oxidative stress-mediated injury induced by D-galactose. *J. Agric. Food Chem.* **2009**, *57*, 7731–7736. Available online: <https://pubmed.ncbi.nlm.nih.gov/19722705/> (accessed on 24 September 2022). [CrossRef]
18. Zhang, Z.F.; Zhang, Y.Q.; Fan, S.H.; Zhuang, J.; Zheng, Y.L.; Lu, J.; Wu, D.M.; Shan, Q.; Hu, B. Troxerutin protects against 2,2',4,4'-tetrabromodiphenyl ether (BDE-47)-induced liver inflammation by attenuating oxidative stress-mediated NAD⁺-depletion. *J. Hazard. Mater.* **2015**, *283*, 98–109. Available online: <https://pubmed.ncbi.nlm.nih.gov/25262482/> (accessed on 24 September 2022). [CrossRef]

19. Casili, G.; Lanza, M.; Campolo, M.; Messina, S.; Scuderi, S.; Ardizzone, A.; Filippone, A.; Paterniti, I.; Cuzzocrea, S.; Esposito, E. Therapeutic potential of flavonoids in the treatment of chronic venous insufficiency. *Vasc. Pharmacol.* **2021**, *137*, 106825. Available online: <https://www.sciencedirect.com/science/article/abs/pii/S153718912030330X?via%3Dihub> (accessed on 24 September 2022). [CrossRef]
20. Boisseau, M.R.; Taccoen, A.; Garreau, C.; Vergnes, C.; Roudaut, M.F.; Garreau-Gomez, B. Fibrinolysis and Hemorheology in Chronic Venous Insufficiency: A Double Blind Study of Troxerutin Efficiency-PubMed. Available online: <https://pubmed.ncbi.nlm.nih.gov/7593149/> (accessed on 24 September 2022).
21. Cui, X.; Zhang, M.; Guan, X.; Yin, L.; Sun, Y.; Fawcett, J.P.; Gu, J. LC-MS-MS determination of troxerutin in plasma and its application to a pharmacokinetic study. *Chromatographia* **2011**, *73*, 165–169. [CrossRef]
22. Troxerutin European Pharmacopoeia (EP) Reference Standard 7085-55-4. Available online: https://www.sigmaaldrich.com/SA/en/product/sial/y0000497?gclid=Cj0KCQjw1bqZBhDXARIsANTjCPLdKv45ZWE_h113biIEYAxhGAb19AT0PMG9zg97_ThJBWSwAKd-ZrUaApiDEALw_wcB&gclid=aw.ds (accessed on 24 September 2022).
23. Najahi-Missaoui, W.; Arnold, R.D.; Cummings, B.S. Safe Nanoparticles: Are We There Yet? *Int. J. Mol. Sci.* **2020**, *22*, 385. Available online: <https://pubmed.ncbi.nlm.nih.gov/33396561/> (accessed on 24 September 2022). [CrossRef] [PubMed]
24. Yetisgin, A.A.; Cetinel, S.; Zuvun, M.; Kosar, A.; Kutlu, O. Therapeutic Nanoparticles and Their Targeted Delivery Applications. *Molecules* **2020**, *25*, 2193. Available online: <https://www.ncbi.nlm.nih.gov/pmc/articles/PMC7248934/> (accessed on 6 August 2022). [CrossRef] [PubMed]
25. Montoto, S.S.; Muraca, G.; Ruiz, M.E. Solid Lipid Nanoparticles for Drug Delivery: Pharmacological and Biopharmaceutical Aspects. *Front. Mol. Biosci.* **2020**, *7*, 319. Available online: <https://pubmed.ncbi.nlm.nih.gov/33195435/> (accessed on 24 September 2022).
26. Souto, E.B.; Doktorová, S. Chapter 6—Solid lipid nanoparticle formulations pharmacokinetic and biopharmaceutical aspects in drug delivery. *Methods Enzym.* **2009**, *464*, 105–129. Available online: <https://pubmed.ncbi.nlm.nih.gov/19903552/> (accessed on 6 August 2022).
27. Tan, M.E.; He, C.H.; Jiang, W.; Zeng, C.; Yu, N.; Huang, W.; Gao, Z.G.; Xing, J.G. Development of solid lipid nanoparticles containing total flavonoid extract from *Dracocephalum moldavica* L. and their therapeutic effect against myocardial ischemia–reperfusion injury in rats. *Int. J. Nanomed.* **2017**, *12*, 3253–3265. Available online: <https://www.dovepress.com/development-of-solid-lipid-nanoparticles-containing-total-flavonoid-ex-peer-reviewed-fulltext-article-IJN> (accessed on 24 September 2022).
28. Zhao, T.; Wu, W.; Sui, L.; Huang, Q.; Nan, Y.; Liu, J.; Ai, K. Reactive oxygen species-based nanomaterials for the treatment of myocardial ischemia reperfusion injuries. *Bioact. Mater.* **2022**, *7*, 47–72. Available online: <https://www.ncbi.nlm.nih.gov/pmc/articles/PMC8377441/> (accessed on 24 September 2022). [CrossRef]
29. Rostami, E.; Kashanian, S.; Azandaryani, A.H.; Faramarzi, H.; Dolatabadi, J.E.; Omidfar, K. Drug targeting using solid lipid nanoparticles. *Chem. Phys. Lipids.* **2014**, *181*, 56–61. Available online: <https://pubmed.ncbi.nlm.nih.gov/24717692/> (accessed on 24 September 2022). [CrossRef]
30. Subbaraj, G.K.; Elangovan, H.; Chandramouli, P.; Yasam, S.K.; Chandrasekaran, K.; Kulanthaivel, L.; Pandi, S.; Subramanian, S. Antiangiogenic Potential of Troxerutin and Chitosan Loaded Troxerutin on Chorioallantoic Membrane Model. *Biomed. Res. Int.* **2023**, *2023*, 5956154. Available online: <https://pubmed.ncbi.nlm.nih.gov/37260851/> (accessed on 24 September 2022). [CrossRef]
31. Saranya, T.; Kavithaa, K.; Paulpandi, M.; Ramya, S.; Winster, S.H.; Mani, G.; Dhayalan, S.; Balachandar, V.; Narayanansamy, A. The creation of selenium nanoparticles decorated with troxerutin and their ability to adapt to the tumour microenvironment have therapeutic implications for triple-negative breast cancer. *New J. Chem.* **2023**, *47*, 4565–4576. Available online: <https://pubs.rsc.org/en/content/articlelanding/2004/yg/d2nj05671b/unauth> (accessed on 1 October 2023). [CrossRef]
32. Zeng, C.; Jiang, W.; Tan, M.; Xing, J.; He, C. Improved Oral Bioavailability of Total Flavonoids of *Dracocephalum moldavica* via Composite Phospholipid Liposomes: Preparation, in-vitro Drug Release and Pharmacokinetics in Rats. *Pharmacogn. Mag.* **2016**, *12*, 313–318. Available online: <https://pubmed.ncbi.nlm.nih.gov/27867275/> (accessed on 1 October 2023).
33. Janakiraman, A.K.; Sumathi, B.; Mohamed Saleem, T.; Ramkanth, S.; Odaya Kumar, P.; Venkatachalam, G. Design and evaluation of Carvedilol nanocrystals sustained release tablets. *J. App. Pharm. Sci.* **2017**, *7*, 61–68.
34. Kumar, V.V.; Chandrasekar, D.; Ramakrishna, S.; Kishan, V.; Rao, Y.M.; Diwan, P.V. Development and evaluation of nitrendipine loaded solid lipid nanoparticles: Influence of wax and glyceride lipids on plasma pharmacokinetics. *Int. J. Pharm.* **2006**, *335*, 167–175. Available online: <https://europepmc.org/article/med/17161566> (accessed on 28 December 2022). [CrossRef] [PubMed]
35. Teeranachaideekul, V.; Souto, E.; Müller, R.; Junyaprasert, V.B. Physicochemical characterization and in vitro release studies of ascorbyl palmitate-loaded semi-solid nanostructured lipid carriers (NLC gels). *J. Microencapsul.* **2008**, *25*, 111–120. Available online: <https://pubmed.ncbi.nlm.nih.gov/18246489/> (accessed on 19 April 2023). [CrossRef] [PubMed]
36. Hwang, K.M.; Byun, W.; Cho, C.H.; Park, E.S. Preparation and optimization of glyceryl behenate-based highly porous pellets containing cilostazol. *Pharm. Dev. Technol.* **2016**, *23*, 540–551. Available online: <https://www.tandfonline.com/doi/abs/10.1080/10837450.2016.1245743> (accessed on 19 April 2023). [CrossRef] [PubMed]
37. Le, N.T.T.; Cao, V.D.; Nguyen, T.N.Q.; Le, T.T.H.; Tran, T.T.; Thi, T.T.H. Soy Lecithin-Derived Liposomal Delivery Systems: Surface Modification and Current Applications. *Int. J. Mol. Sci.* **2019**, *20*, 4706. Available online: <https://pubmed.ncbi.nlm.nih.gov/31547569/> (accessed on 19 April 2023). [CrossRef] [PubMed]

38. Genç, L. Preparation and characterization of nocodazole-loaded solid lipid nanoparticles. *Pharm. Dev. Technol.* **2013**, *19*, 671–676. Available online: <https://www.tandfonline.com/doi/abs/10.3109/10837450.2013.819017> (accessed on 19 April 2023). [CrossRef]
39. Kumar, A.J.; Ramkanth, S.; Lakshmana, S.P.; Gopal, V. Enhancement of saturation solubility and in vitro dissolution of carvedilol nanoparticles by high pressure homogenization technique. *Int. J. Curr. Pharm. Rev. Res.* **2015**, *6*, 269–273.
40. Danaei, M.; Dehghankhold, M.; Ataei, S.; Hasanzadeh, F.D.; Javanmard, R.; Dokhani, A.; Mozafari, M.R. Impact of Particle Size and Polydispersity Index on the Clinical Applications of Lipidic Nanocarrier Systems. *Pharmaceutics* **2018**, *10*, 57. Available online: <https://pubmed.ncbi.nlm.nih.gov/29783687/> (accessed on 2 April 2023). [CrossRef]
41. Surface Area to Volume Ratio in Nanoparticles | Winner Science. Available online: <https://winnerscience.com/surface-area-to-volume-ratio-in-nanoparticles/> (accessed on 10 May 2023).
42. The Effect of Rice Bran Wax on Physicochemical Properties of Curcuminoid-Loaded Solid Lipid Nanoparticles. Available online: https://www.researchgate.net/publication/305432628_The_effect_of_rice_bran_wax_on_physicochemical_properties_of_curcuminoidloaded_solid_lipid_nanoparticles#pf3 (accessed on 2 April 2023).
43. Satyanarayana, S.D.; Lila, A.S.A.; Moin, A.; Moglad, E.H.; Khafagy, E.S.; Alotaibi, H.F.; Obaidullah, A.J.; Charyulu, R.N. Ocular Delivery of Bimatoprost-Loaded Solid Lipid Nanoparticles for Effective Management of Glaucoma. *Pharmaceutics* **2023**, *16*, 1001. [CrossRef]
44. Suhaimi, S.H.; Hasham, R.; Rosli, N.A. Akademia Baru Effects of Formulation Parameters on Particle Size and Polydispersity Index of Orthosiphon Stamineus Loaded Nanostructured Lipid Carrier. *J. Adv. Res. Appl. Sci. Eng. Technol.* **2015**, *1*, 36–39.
45. Devaraj, P.; Kumari, P.; Aarti, C.; Renganathan, A. Synthesis and characterization of silver nanoparticles using cannonball leaves and their cytotoxic activity against MCF-7 cell line. *J. Nanotechnol.* **2013**, *2013*, 598328. [CrossRef]
46. Musielak, E.; Feliczak-Guzik, A.; Nowak, I. Optimization of the Conditions of Solid Lipid Nanoparticles (SLN) Synthesis. *Molecules* **2022**, *27*, 2202. [CrossRef] [PubMed]
47. Hu, L.; Xing, Q.; Meng, J.; Shang, C. Preparation and Enhanced Oral Bioavailability of Cryptotanshinone-Loaded Solid Lipid Nanoparticles. *AAPS PharmSciTech* **2010**, *11*, 582. Available online: <https://www.ncbi.nlm.nih.gov/pmc/articles/PMC2902353/> (accessed on 4 April 2023). [CrossRef] [PubMed]
48. Singh, S.; Kamal, S.S.; Sharma, A.; Kaur, D.; Katual, M.K.; Kumar, R. Formulation and In-Vitro Evaluation of Solid Lipid Nanoparticles Containing Levosulpiride. *Open Nanomed. J.* **2017**, *4*, 17–29. [CrossRef]
49. Shinde, G.; Shiyani, S.; Shelke, S.; Chouthe, R.; Kulkarni, D.; Marvaniya, K. Enhanced brain targeting efficiency using 5-FU (fluorouracil) lipid–drug conjugated nanoparticles in brain cancer therapy. *Prog. Biomater.* **2020**, *9*, 259–275. Available online: <https://link.springer.com/article/10.1007/s40204-020-00147-y> (accessed on 4 April 2023). [CrossRef] [PubMed]
50. Winey, M.; Meehl, J.B.; O’Toole, E.T.; Giddings, T.H. Conventional transmission electron microscopy. *Mol. Biol. Cell* **2014**, *25*, 319. Available online: <https://www.ncbi.nlm.nih.gov/pmc/articles/PMC3907272/> (accessed on 16 April 2023). [CrossRef] [PubMed]
51. Ulusoy, U. A Review of Particle Shape Effects on Material Properties for Various Engineering Applications: From Macro to Nanoscale. *Minerals* **2023**, *13*, 91. Available online: <https://www.mdpi.com/2075-163X/13/1/91/html> (accessed on 16 April 2023). [CrossRef]
52. Pagar, R.R.; Musale, S.R.; Pawar, G.; Kulkarni, D.; Giram, P.S. Comprehensive Review on the Degradation Chemistry and Toxicity Studies of Functional Materials. *ACS Biomater. Sci. Eng.* **2022**, *8*, 2161–2195. Available online: <https://pubs.acs.org/doi/abs/10.1021/acsbiomaterials.1c01304> (accessed on 22 September 2022). [CrossRef]

Disclaimer/Publisher’s Note: The statements, opinions and data contained in all publications are solely those of the individual author(s) and contributor(s) and not of MDPI and/or the editor(s). MDPI and/or the editor(s) disclaim responsibility for any injury to people or property resulting from any ideas, methods, instructions or products referred to in the content.